Mathematical Biosciences and Engineering

MBE, 19(4): 3487–3508.
DOI: 10.3934/mbe.2022161
Received: 07 December 2021
Revised: 12 January 2022
Accepted: 18 January 2022
Published: 27 January 2022

http://www.aimspress.com/journal/MBE

Research article

Nonlinear saturation controller simulation for reducing the high vibrations of a dynamical system

Hany Bauomy[1,2,*] and Ashraf Taha[3]

[1] Department of Mathematics, College of Arts and Science in Wadi Addawasir, Prince Sattam Bin Abdulaziz University, P.O. Box 54, Wadi Addawasir 11991, Saudi Arabia
[2] Department of Mathematics, Faculty of Science, Zagazig University, Zagazig 44519, Egypt
[3] Department of Basic Sciences, Modern Academy for Engineering and Technology, El-Hadaba El-Wosta, Elmokattam 11585, Egypt

* **Correspondence:** Email: hany_samih@yahoo.com.

Abstract: This paper studies the nonlinear vibrating behaviour of a nonlinear cantilever beam system (primary system) using a nonlinear absorber (the secondary system). The nonlinear vibrating behavior for the present dynamical system is considered with the effect of the external force. The one controller type, nonlinear saturation controller (NSC), is introduced to decrease the vibration of this system. Perturbation method treatment is produced to get the mathematical solution of the equations for the dynamical modeling with NSC. The perturbation technique is used to obtain the approximate solution of the dynamical system. This research focuses on resonance case with primary and 1:2 internal resonance. Time histories of the primary system and the controller are shown to demonstrate the reaction with and without control. The time-history response, as well as the impacts of the parameters on the system and controller, are simulated numerically using the MATLAB program. Routh-Hurwitz criterion is used to examine the stability of the system under primary resonance. A numerical simulation, using the MATLAB program, is obtained to show the time-history response, the effect of the parameters on the system and the controller. The effects of system parameters on the performance of the primary system and the controller are investigated. A comparison between all the obtained solutions made to confirm the results. Validation curves are provided to show how closely the perturbation and numerical solutions are related. A comparison is made with recently released papers.

Keywords: perturbation technique; nonlinear saturation controller; stability; resonance case;

external excitation

1. Introduction

In recent years, applications of controllers using the saturation phenomenon developed to end system's vibrations. Many researchers studied this phenomenon in different dynamical systems. Oueini et al. [1] recommended an active control for a cantilever beam by adding a vibration damper. The flexible structure with the controller has been presented analytically using multiple scale method at two-to-one autoparametric resonances. Pai et al. [2] improved the performance of NSC and the linear position feedback algorithm analytically, numerically and experimentally. From this study they showed that NSC is efficient to decrease the steady-state vibrations. Oueini and Nayfeh [3] a control strategy for the excited beam by cubic velocity feedback under a principal parametric resonance is suggested. The analysis detected that this controller reduced the amplitude of the response. Pai and Schulz [4] introduced a controller connected to a system with quadratic terms depended on saturation occurrence. They controlled the oscillation of the system via PZT patches as actuators and sensor. Pai et al. [5] considered some absorbers depended on saturation phenomena designed in support of declining the vibrations of a plate model. Ashour and Nayfeh [6] used an absorber based on saturation phenomena for lessening vibrations of the model. In favor of raising the action of the saturation control they determine the frequency of excitation together with the system. Jun et al. [7] illustrated the saturation controller to the structure by processing typical PZT patches. Depended on analytical solutions these authors showed that the nonlinear absorber (NSC) was globally stable, as distinct from a linear model where growing feedback gain value might instead go in front to instability. However, for a nonlinear absorber, the power need will be greater than that for the linear system. Jun et al. [8] presented a nonlinear saturation controller for decreasing vibrations of a self-excited plant. The control mechanism performed via combination the absorber among the plant applying quadratic nonlinearity. Xu et al. [9] proposed the influence of a time-delay in a structure depending of a linear beam with NSC absorber. The analytical results based on the multiple scales method revealed much more complex dynamics for the system. Presence of the time-delay widened or decreased the frequency bandwidth of effective vibration suppuration.

EL-Sayed [10] presented the purpose delay positive position feedback control (DPPF) in support of reduction vibrations in the Van der Pol oscillators system with external forces. The effectiveness of vibrations suppuration by DPPF is tested for selected parameters to obtain the stability condition of the model. Warminski et al. [11] concentrated on appliance of special controllers for a flexible beam with MFC actuators. Mathematical solutions for the beam with NSC obtained using perturbation technique. The best controllers for reduction the vibration for the system are NSC and PPF controllers. Saeed et al. [12] illustrated time-delay saturation controller to decrease oscillations of nonlinear beam. Hamed, and Elagan [13] considered effeteness of NSC control algorithms for huge oscillation of the beam structure. Hamed and Amer [14] used NSC to decrease the oscillation amplitude of a composite beam. Kamel et al. [15] proposed a magnetically levitated body with a NSC to decrease the horizontal vibration simulated by a nonlinear differential equation. Omidi and Mahmoodi [16] for nonlinear oscillation decreasing, they performed the Positive Position Feedback (PPF), the Integral Resonant Control (IRC) and Nonlinear Integral Positive Position Feedback (NIPPF). They solved analytically the system using multiple scales method. Conclusions show that controller construct has mainly job in

suppression performance.

Numerous main papers are studied the vibration absorbers on various nonlinear systems. Linear and nonlinear dynamic vibration absorbers have been employed to suppress the primary resonance vibrations of a weakly nonlinear oscillator systems having cubic nonlinearity subjected to external excitations under primary resonance conditions [17–20]. The method of multiple scales is used to obtain the averaged equations that determine the amplitudes and phases of the first-order approximate solutions to the vibrations of the primary nonlinear oscillator and nonlinear absorber. The nonlinear absorber can effectively suppress the amplitude of primary resonance response and eliminate saddle-node bifurcations occurring in the frequency-response curves of the primary nonlinear oscillator. Numerical results are given to show the effectiveness of the nonlinear absorber for suppressing nonlinear vibrations of the primary nonlinear oscillator under primary resonance conditions. Moreover, different control approaches are investigated and confirmed to decrease the unsafe vibrations which are made in different nonlinear systems [21–25]. Furthermore, Ji et al. [26] studied the dynamic behavior of a quadratic nonlinear oscillator involving time delay under two-to-one resonances of two Hopf bifurcations. Also, Ji [27] investigated the secondary resonance response of a time-delayed quadratic nonlinear oscillator after the trivial equilibrium of the system loses its stability via two-to-one resonant Hopf bifurcations. Zhang and Li [28] investigated the global bifurcations and chaotic dynamics of a nonlinear oscillator with two-degree-of-freedom. The fast and slow modes may exist simultaneously, and the chaotic motions were found by using numerical simulation. Chaos in beams has been widely investigated recently. With the Galerkin method, the method of multiple scales and numerical simulations, Zhang [29] investigated the chaotic motion and its control for the nonlinear non-planar oscillations of a cantilever beam subjected to a harmonic axial excitation and transverse excitations at the free end. By means of the Galerkin procedure, normal form theory and a global perturbation method. Zhang et al. [30] investigated the bifurcations and chaotic dynamics of a simply support symmetric cross-ply composite laminated piezoelectric rectangular plate, which are simultaneously forced by the transverse and in-plane excitations and the excitation loaded by the piezoelectric layers. Hao et al. [31] studied the complicated nonlinear dynamics of a functionally graded material cantilever rectangular plate subjected to the transverse excitation in thermal environment. Zhang et al. [32] analyzed nonlinear dynamic responses of cantilever rectangular laminates with external excitation. Nonlinear forced vibration characteristics of carbon nanotube reinforced composite plates were studied by Guo and Zhang [33]. Lu et al. [34] proposed a robust control method for the vibration suppression of composite laminated cantilever rectangular plates subjected to the aerodynamic force in hygrothermal environment. Recently, Siriguleng et al. [35] studied the dynamic response of a rotating laminated composite blade in the case of 2:1 internal resonance and the author reported the interesting saturation phenomena in the rotating composite blade.

The key goal of this research is to provide a general guideline for removing high vibrations of the framework by using a suitable control technique. The nonlinear saturation control (NSC) considered for active suppression of high vibration for the nonlinear dynamical system which presented in [16]. The analytical result received by using perturbation technique process near simultaneous internal and primary resonance case. The comprehensive mathematical solutions, frequency response equations (FREs), and stability analysis with NSC process are obtained using the perturbation method. Numerical solution and effect of all parameters on the vibrating system and NSC system are plotted and reported. The MATLAB software is used to simulate the impact of various parameters and the controller on the system. The validations of the analysis's time history and frequency response curves (FRCs), as well

as the numerical results, were satisfied by comparing them. Before and after providing the controller in the simultaneous internal and primary resonance case, the system is numerically and graphically examined. The simulation outcomes give that the NSC method is found to be the most effective at eliminating high vibrations and making the system more stable. Finally, numerical results are obtained that show an outstanding agreement per the analytical results.

2. Governing equations and approximate solutions

In this section, the model for the nonlinear dynamics of a cantilever beam is governed by a nonlinear partial differential equation. The primary resonant mode of the cantilever beam is considered not to be involved in an internal resonance with other modes of the system. Single-mode discretization approach results in nonlinear differential equation of [16] yields:

$$\ddot{x} + \eta_s \dot{x} + \omega_s^2 x + \alpha x^3 + \beta x \dot{x}^2 + \gamma x^2 \dot{x} = f \cos(\Omega t) \tag{2.1}$$

To perform the multiple-time-scale procedure, system parameters are scaled, such that:

$$\eta_s \to \varepsilon \eta_s,\ \alpha \to \varepsilon \alpha,\ \beta \to \varepsilon \beta,\ \gamma \to \varepsilon \gamma,\ f \to \varepsilon f$$

So, the equation motion of the cantilever beam obtained from [16] is modified by using NSC process as follows:

$$\ddot{x} + \varepsilon \eta_s \dot{x} + \omega_s^2 x + \varepsilon \alpha x^3 + \varepsilon \beta x \dot{x}^2 + \varepsilon \gamma x^2 \dot{x} = \varepsilon\, f \cos(\Omega t) + \varepsilon \gamma_1\ v^2 \tag{2.2}$$

$$\ddot{v} + \varepsilon \eta_c \dot{v} + \omega_c^2 v\ = \varepsilon \gamma_2\, x\, v \tag{2.3}$$

where η_s and η_c are linear damping coefficients of the main system and NSC, f and Ω are the forcing amplitude and the frequency of the system, ω_s and ω_c are natural frequencies of the main system and NSC, α, β and γ are nonlinear factors, γ_1 is control signal gain, γ_2 is feedback signal gain and ε is a small perturbation value.

Figure 1 shows connection of NSC system to the main system in a closed figure which describing Eqs (2.2) and (2.3).

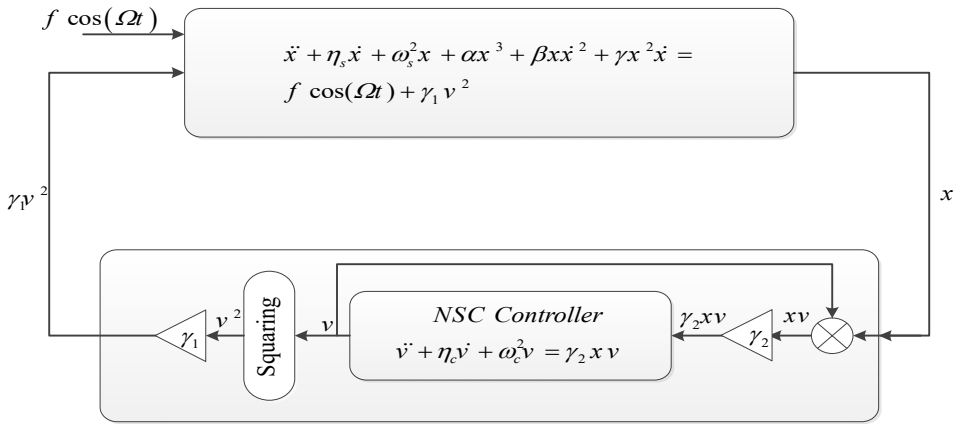

Figure 1. Block map of the blocked loop system.

2.1. Perturbation analysis

In this section, the perturbation manner [36,37] is useful to seek the approximate solutions of Eqs (2.2) and (2.3) as known:

$$x(t,\varepsilon)=x_0(T_0,T_1)+\varepsilon x_1(T_0,T_1)+O(\varepsilon^2) \tag{2.4}$$

$$v(t,\varepsilon)=v_0(T_0,T_1)+\varepsilon v_1(T_0,T_1)+O(\varepsilon^2) \tag{2.5}$$

The time derivatives of the Eqs (2.2) and (2.3) can be written in terms of two time-scales as:

$$\frac{d}{dt}=D_0+\varepsilon D_1,\ \ \frac{d^2}{dt^2}=D_0^2+\varepsilon(2D_0D_1),\ \ D_n=\frac{\partial}{\partial \mathrm{T}_n}\ (n=0,1) \tag{2.6}$$

Inserting Eqs (2.4) to (2.6) in Eqs (2.2) and (2.3), and compare coefficients of similar power of ε, we achieve:

$O(\varepsilon^0)$:

$$\left(D_0^2+\omega_s^2\right)x_0=0 \tag{2.7}$$

$$\left(D_0^2+\omega_c^2\right)v_0=0 \tag{2.8}$$

$O(\varepsilon^1)$:

$$\left(D_0^2+\omega_s^2\right)x_1=-2D_1D_0x_0-\eta_sD_0x_0-\alpha x_0^3-\beta x_0\left(D_0x_0\right)^2-\gamma x_0^2D_0x_0+f\cos(\Omega t)+\gamma_1v_0^2 \tag{2.9}$$

$$\left(D_0^2+\omega_c^2\right)v_1=-2D_1D_0v_0-\eta_cD_0v_0+\gamma_2x_0v_0 \tag{2.10}$$

The solutions of Eqs (2.7) and (2.8) are:

$$x_0 = A_1(T_0,T_1)\exp(i\,\omega_s T_0) + cc. \tag{2.11}$$

$$v_0 = A_2(T_0,T_1)\exp(i\,\omega_c T_0) + cc. \tag{2.12}$$

Where, $A_1(T_0,T_1)$, $A_2(T_0,T_1)$ are complex functions in T_0 and T_1, $cc.$ locate for the complex conjugate of the preceding terms. Substitute Eqs (2.11) and (2.12) interested in Eqs (2.9) and (2.10), we obtain the following solutions:

$$x_1 = \left[\frac{\alpha A_1^3 - \beta\omega_s^2 A_1^3 - \gamma\omega_s^2 A_1^3}{8\omega_s^2}\right]\exp(3i\,\omega_s T_0) + \left[\frac{f}{2\left(\omega_s^2 - \Omega^2\right)}\right]\exp(i\,\Omega T_0) + \left[\frac{\gamma_1 A_2^2}{\omega_s^2 - 4\omega_c^2}\right]\exp(2i\,\omega_c T_0)$$
$$+ \left[\frac{\gamma_1 A_2 \bar{A}_2}{\omega_s^2}\right] + cc. \tag{2.13}$$

$$v_1 = \left[\frac{\gamma_2 A_1 A_2}{\omega_c^2 - \left(\omega_s + \omega_c\right)^2}\right]\exp(i\,\left(\omega_s + \omega_c\right)T_0) + \left[\frac{\gamma_2 A_1 \bar{A}_2}{\omega_c^2 - \left(\omega_s - \omega_c\right)^2}\right]\exp(i\,\left(\omega_s - \omega_c\right)T_0) + cc. \tag{2.14}$$

Wherever the over bar indicates the complex conjugate function. Before we proceed to the next step of the solution, we have to establish the possible resonance cases at Eqs (2.13) and (2.14) which be primary resonance ($\Omega \cong \omega_s$), internal resonance ($\omega_s \cong 2\omega_c$), and simultaneous resonance ($\Omega \cong \omega_s$, $\omega_s \cong 2\omega_c$) that is the worst one. Therefore, this case is investigated by introducing the two parameters σ_1 and σ_2 to describe quantitatively the closeness of Ω and ω_c to ω_s as follows:

$$\Omega \cong \omega_s + \varepsilon\sigma_1,\ \omega_s \cong 2\omega_c + \varepsilon\sigma_2 \tag{2.15}$$

Inserting Eq (2.15) into the small-divisor and secular terms of Eqs (2.9) and (2.10), we get the following solvability conditions:

$$2i\,\omega_s D_1 A_1 = \left[-i\,\omega_s\eta_s A_1 + \left(-3\alpha - \beta\omega_s^2 + 3\gamma\omega_s^2\right)A_1^2\bar{A}_1\right]$$

$$+\left[\frac{f}{2}\right]\exp(i\,\sigma_1 T_1) + \left[\gamma_1 A_2^2\right]\exp(-i\,\sigma_2 T_1) \tag{2.16}$$

$$2i\,\omega_c D_1 A_2 = -i\,\omega_c\eta_c A_2 + \gamma_2 A_1\bar{A}_2\exp(i\,\sigma_2 T_1) \tag{2.17}$$

For analyzing Eqs (2.16) and (2.17), we rewrite $A_1(T_1)$ and $A_2(T_1)$ in polar form as follows:

$$A_n = \frac{1}{2} a_n \exp(i\,\beta_n), \qquad n = 1,2 \tag{2.18}$$

Wherever, a_1 and a_2 are the steady-state amplitudes of the system and β_1, β_2 are the phases of the two motions. Applying Eq (2.18) into Eqs (2.16) and (2.17) and sorting out the real and imaginary parts, we acquire the following set of first-order differential equations.

$$\dot{a}_1 = -\frac{\eta_s}{2} a_1 + \left[\frac{f}{2\omega_s}\right]\sin(\theta_1) + \left[-\frac{\gamma_1}{4\omega_s} a_2^2\right]\sin(\theta_2) \tag{2.19}$$

$$a_1\dot{\beta}_1 = \left(\frac{3\alpha}{8\omega_s} + \frac{\beta\omega_s}{8} - \frac{3\gamma\omega_s}{8}\right)a_1^3 + \left[-\frac{f}{2\omega_s}\right]\cos(\theta_1) + \left[-\frac{\gamma_1}{4\omega_s} a_2^2\right]\cos(\theta_2) \tag{2.20}$$

$$\dot{a}_2 = -\frac{\eta_c}{2} a_2 + \left[\frac{\gamma_2}{4\omega_c} a_1 a_2\right]\sin(\theta_2) \tag{2.21}$$

$$a_2\dot{\beta}_2 = \left[-\frac{\gamma_2}{4\omega_c} a_1 a_2\right]\cos(\theta_2) \tag{2.22}$$

Where, $\theta_1 = \sigma_1 T_1 - \beta_1$, and $\theta_2 = \sigma_2 T_1 + \beta_1 - 2\beta_2$.

Equations (2.19) to (2.22) form the system amplitude-phase modulating equations.

3. Stability analysis

The variations of amplitudes and phases of a periodically excited system are zero at steady state. So, the algebraic equations that govern the steady state vibrations of the considered structure can be found from Eqs (2.19) to (2.22) by setting $\dot{a}_1 = \dot{a}_2 = \dot{\theta}_1 = \dot{\theta}_2 = 0$, yields

$$\frac{\eta_s}{2} a_1 = \left[\frac{f}{2\omega_s}\right]\sin(\theta_1) - \left[\frac{\gamma_1}{4\omega_s} a_2^2\right]\sin(\theta_2) \tag{3.1}$$

$$a_1\sigma_1 - \left(\frac{3\alpha}{8\omega_s} + \frac{\beta\omega_s}{8} - \frac{3\gamma\omega_s}{8}\right)a_1^3 = -\left[\frac{f}{2\omega_s}\right]\cos(\theta_1) - \left[\frac{\gamma_1}{4\omega_s} a_2^2\right]\cos(\theta_2) \tag{3.2}$$

$$\frac{\eta_c}{2} a_2 = \left[\frac{\gamma_2}{4\omega_c} a_1 a_2\right]\sin(\theta_2) \tag{3.3}$$

$$\frac{a_2}{2}\left(\sigma_2 + \sigma_1\right) = -\left[\frac{\gamma_2}{4\omega_c} a_1 a_2\right]\cos(\theta_2) \tag{3.4}$$

From Eqs (3.1) to (3.4) we have the following cases:

(I) $a_1 \neq 0, a_2 = 0$ (II) $a_2 \neq 0, a_1 = 0$ and (III) $a_1 \neq 0, a_2 \neq 0$.

In support of the helpful case (III), Squaring Eqs (3.1) and (3.2), after that count the squared results together, similarly do the same for Eqs (3.3) and (3.4), next we contain the successive frequency response equations:

$$\frac{\eta_c^2}{4} + \frac{1}{4}\left(\sigma_2 + \sigma_1\right)^2 = \frac{\gamma_2^2}{16\omega_c^2} a_1^2 \tag{3.5}$$

$$\left(\frac{\eta_s}{2} a_1 + \frac{\omega_c \eta_c \gamma_1 a_2^2}{2\gamma_2 \omega_s a_1}\right)^2 + \left(a_1\sigma_1 - \left(\frac{3\alpha}{8\omega_s} + \frac{\beta\omega_s}{8} - \frac{3\gamma\omega_s}{8}\right)a_1^3 - \frac{\gamma_1\omega_c}{2\omega_s\gamma_2 a_1} a_2^2\left(\sigma_2 + \sigma_1\right)\right)^2 = \frac{f^2}{4\omega_s^2} \tag{3.6}$$

To perform stability criteria, we assume $a_{10}, a_{20}, \theta_{10}$ and θ_{20} are the solutions of Eqs (3.1) to (3.4), and to observe the performance of small perturbations $a_{11}, a_{21}, \theta_{11}$ and θ_{21} from the steady state solution $a_{10}, a_{20}, \theta_{10}$ and θ_{20} , we let

$$\left.\begin{aligned} &a_1 = a_{11} + a_{10}, \quad a_2 = a_{21} + a_{20}, \quad \theta_1 = \theta_{11} + \theta_{10}, \quad \theta_2 = \theta_{21} + \theta_{10} \\ &\dot{a}_1 = \dot{a}_{11}, \quad \dot{a}_2 = \dot{a}_{21}, \quad \dot{\theta}_1 = \dot{\theta}_{11}, \quad \dot{\theta}_2 = \dot{\theta}_{21} \end{aligned}\right\} \tag{3.7}$$

Substituting Eq (3.7) into Eqs (2.19) to (2.22) and expanding for little parameters $a_{11}, a_{21}, \theta_{11}$ and θ_{21} with carry on linear terms only. We compact the linear system that is equivalent to Eqs (2.19) to (2.22) at the equilibrium point $(a_{10}, a_{20}, \theta_{10}, \theta_{20})$:

$$\begin{bmatrix} \dot{a}_{11} \\ \dot{\theta}_{11} \\ \dot{a}_{21} \\ \dot{\theta}_{21} \end{bmatrix} = \begin{bmatrix} r_{11} & r_{12} & r_{13} & r_{14} \\ r_{21} & r_{22} & r_{23} & r_{24} \\ r_{31} & r_{32} & r_{33} & r_{34} \\ r_{41} & r_{42} & r_{43} & r_{44} \end{bmatrix} \begin{bmatrix} a_{11} \\ \theta_{11} \\ a_{21} \\ \theta_{21} \end{bmatrix} \tag{3.8}$$

Wherever the over matrix is the system Jacobian matrix, and its coefficients are prearranged in the Appendix. One could be able to get the following eigenvalue equations:

$$\begin{vmatrix} r_{11} - \lambda & r_{12} & r_{13} & r_{14} \\ r_{21} & r_{22} - \lambda & r_{23} & r_{24} \\ r_{31} & r_{32} & r_{33} - \lambda & r_{34} \\ r_{41} & r_{42} & r_{43} & r_{44} - \lambda \end{vmatrix} = 0 \tag{3.9}$$

By expanding determinant at Eq (3.9), yields

$$\lambda^4 + \zeta_1\lambda^3 + \zeta_2\lambda^2 + \zeta_3\lambda + \zeta_4 = 0 \tag{3.10}$$

where λ is the eigenvalue of the matrix, $\zeta_1, \zeta_2, \zeta_3$ and ζ_4 are the coefficients of Eq (3.10) known in the Appendix. By applying Routh-Hurwitz criterion for stability, we find the necessary and sufficient conditions to be stable solution are:

$$\zeta_1 > 0, \quad \zeta_1\zeta_2 - \zeta_3 > 0, \quad \zeta_3(\zeta_1\zeta_2 - \zeta_3) - \zeta_1^2\zeta_4 > 0, \quad \zeta_4 > 0 \tag{3.11}$$

4. Numerical simulation results

In this part, the original system Eqs (2.2) and (2.3) are plotted via Runge-Kutta algorithm (by MATLAB 7.14 (R2012a) package) numerically. Figure 2 shows the responses of the model without control process at primary resonance $\Omega \cong \omega_s$ (one of worse resonance cases) and zero initial. This shape appears that, amplitude of the system x regarding 829% of the excitation amplitude f . Figure 3 demonstrate response and phase-plane for the nonlinear dynamical system with NSC at the simultaneous resonance case $\Omega \cong \omega_s$, $2\omega_c \cong \omega_s$ within the initial values $x(0) = 0, \dot{x}(0) = 0, \dot{v}(0) = 0$ and $v(0) = 0.5$. The amplitudes of the system (x) and NSC (v) be about 285.6 and 1,394.2% of the excitation amplitude f , respectively. The saturation appears for the main system and the controller at (t = 700 sec) and (t = 600 sec), correspondingly. It is importance to note that from Figures 2 and 3 the steady state amplitude of the system with NSC condensed to about 65.55 % from its value without NSC. This wealth that the effectiveness of the NSC (E_a = the amplitude of the system without controller / the amplitude of the system with controller) regarding 290.27 for the main system (x).

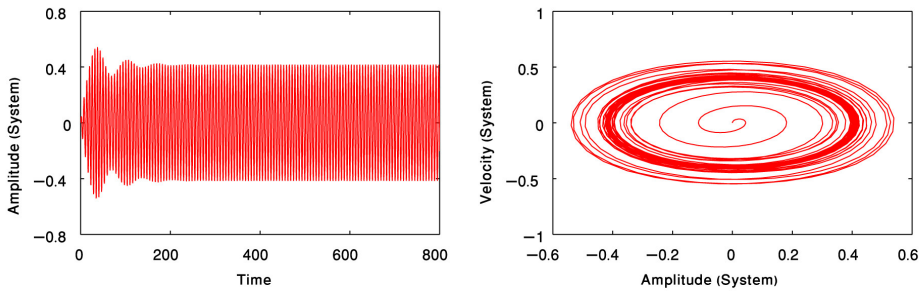

Figure 2. Response of the system with no controller at primary resonance case

($\eta_s = 0.02; \omega_s = 1; \alpha = 0.894; \beta = 0.0001; \gamma = 0.0001; f = 0.05; \Omega \cong \omega_s$).

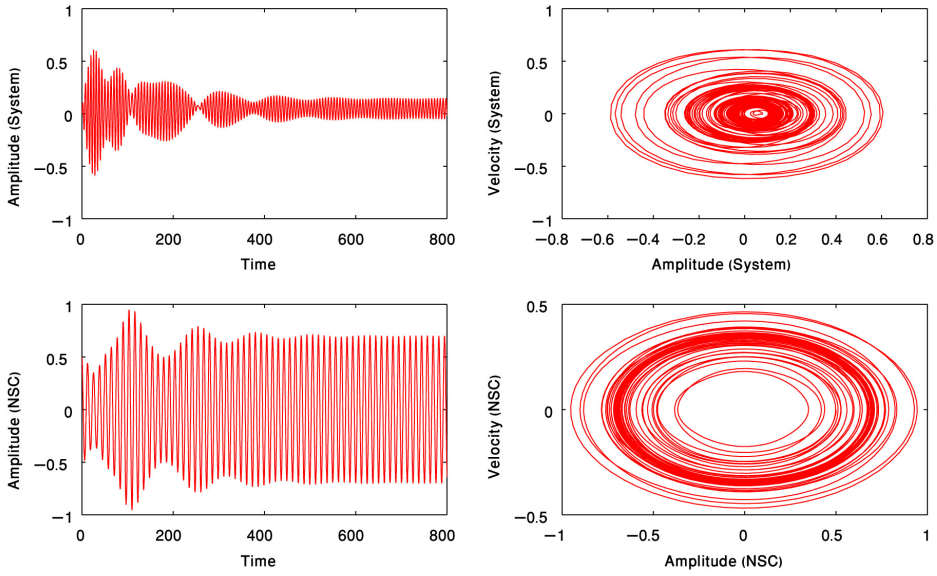

Figure 3. Response of the system and NSC at simultaneous resonance case $\left(\begin{matrix}\eta_s = 0.02; \omega_s = 1; \alpha = 0.894; \beta = 0.0001; \gamma = 0.0001; f = 0.05; \\ \Omega \cong \omega_s; \gamma_1 = 0.2; \eta_c = 0.0001; 2\omega_c = \omega_s; \gamma_2 = 0.1\end{matrix}\right)$.

4.1. The effects of various parameters

In this branch, we will confirm all effect happening in the parameters of the model with NSC near the measured resonance case. The frequency response equations (FRE) specified by Eqs (3.5) and (3.6) solved and plotted by matching value of parameters which showing in Figures 2 and 3. Figure 4 shows the amplitudes for the system and NSC a and b against detuning value σ_1 as surface plot. In Figure 5(a), we presented the frequency response curves in two-dimensional to explain the behavior of the main system (a) before and after NSC (b) at different values of σ_1 on case ($a \neq 0,\ b \neq 0$), moreover, the solid line locate for stable solution and the dashed line for unstable solution. Figure 5(b) indicates bending to the left, it shows obvious soft spring characteristics dominates nonlinearity. Figure 5 shows the frequency–response curves for closed loop case (controller in action) at chosen values to remove the overload risk on the controller for some negative values of detuning parameter σ_1. The figure shows that, the controller work effectively to suppress the main system vibrations at specific frequency bandwidth around σ_1 = 0:0, otherwise the controller will be deactivated automatically.

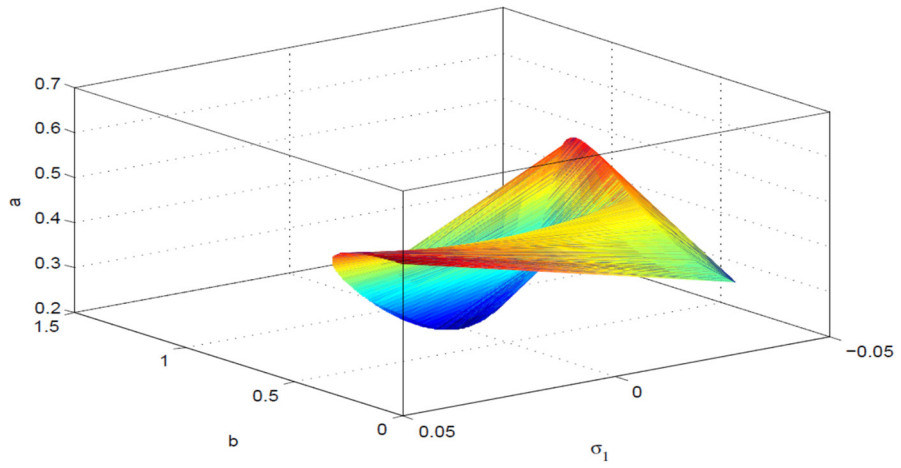

Figure 4. The steady-state amplitudes of system and NSC with the detuning parameter.

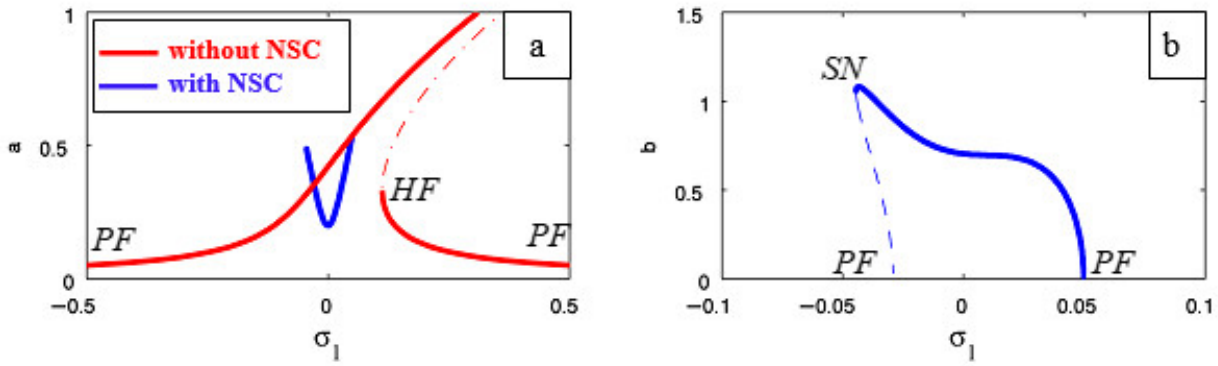

Figure 5. Frequency-response curves (a) the main system a ; (b) NSC b , PF= pitchfork bifurcation, SN= saddle-node bifurcation, and HF= Hopf bifurcation.

4.1.1. Effect of excitation amplitude *f*

Figure 6, explain that the amplitudes of the system and NSC are monotonic increasing functions of the force amplitude *f*. The non-zero solutions at $\sigma_1 = 0$ for the main system are the same when the force is increasing as shown in Figure 6(a–c).

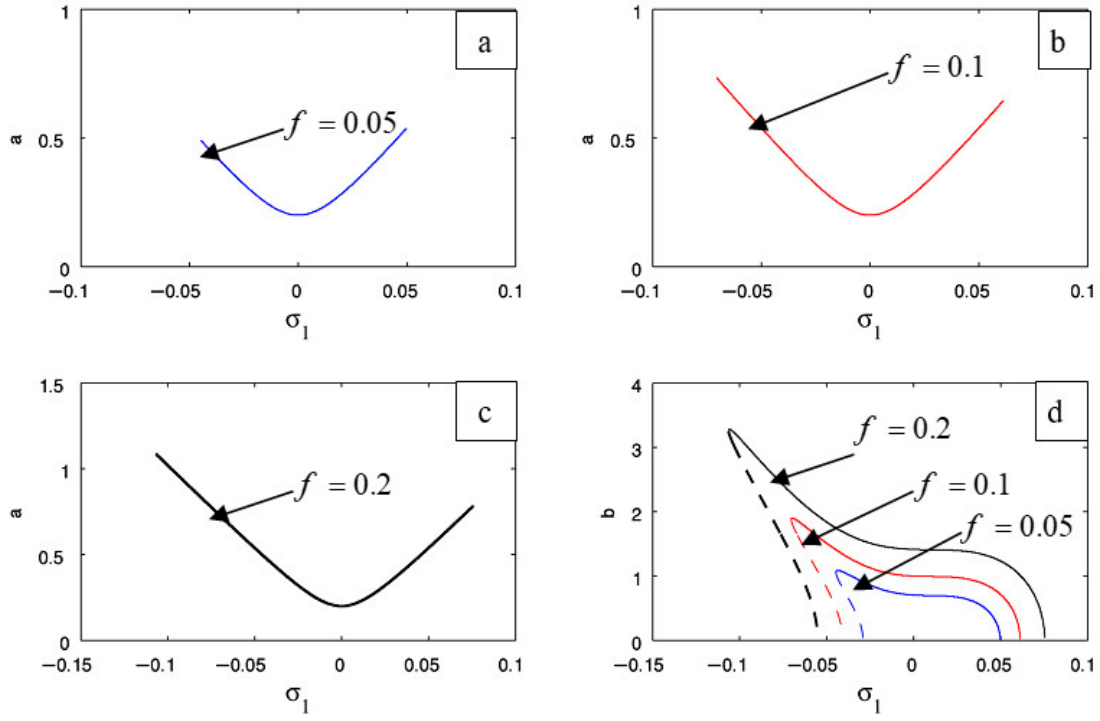

Figure 6. Effects of excitation force f : (a) the main system a ; (b) NSC b .

4.1.2. Effects of linear damping coefficient η_s

On behalf of growing or lessening values for linear damping coefficient η_s the amplitudes of the system and NSC are trivial as seen in Figure 7.

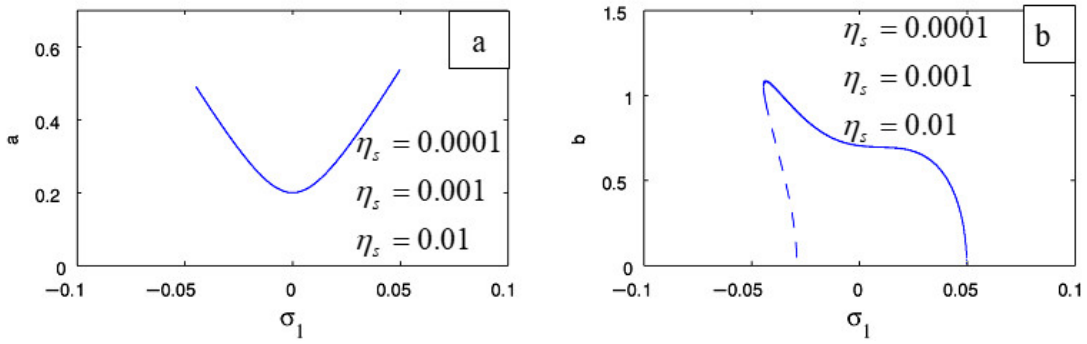

Figure 7. Effects of damping coefficient η_s : (a) the main system a ; (b) NSC b .

4.1.3. Produce of linear damping coefficient η_c and natural frequency ω_s

From Figures 8 and 9, it is seen that the amplitudes of the system and NSC are monotonic lessening

functions in linear damping coefficient η_c and natural frequency ω_s. But at $\sigma_1 = 0$, the amplitude of the system is increasing as exposed in Figures 8(a) and 9(a). Furthermore, the steady state amplitude of NSC is shifting to the left when the natural frequency ω_s increased as shown in Figure 9(b).

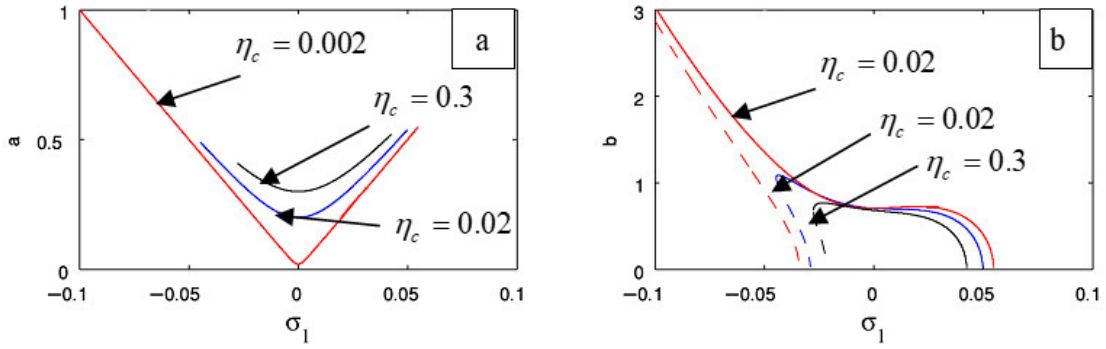

Figure 8. Effects of damping coefficient η_c: (a) the main system a; (b) NSC b.

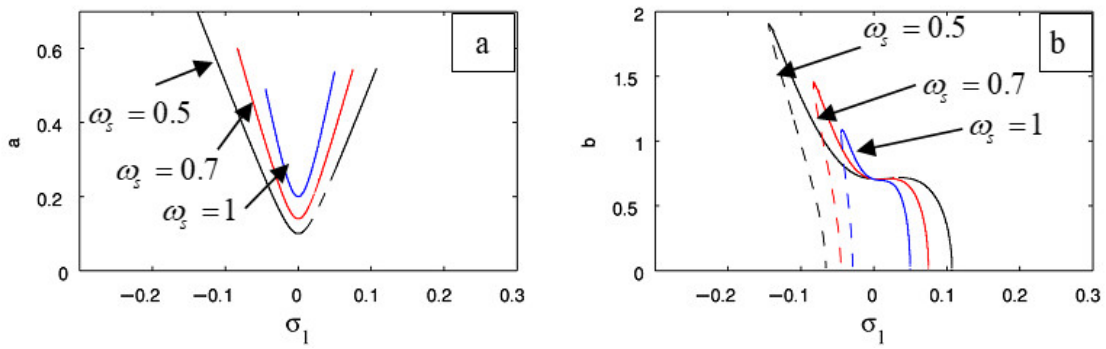

Figure 9. Effects of natural frequency ω_s: (a) the main system a; (b) NSC b.

4.1.4. The effects of nonlinear parameters α, β and γ

It can expected from Figures 10–12 that, as the nonlinear parameters α, β and γ increased, the amplitudes of both system and NSC decreased. Additionally, the frequency bandwidth around $\sigma_1 = 0$ unchanged for the main system as shown in Figures 10(a–c), 11(a–c) and 12(a–c).

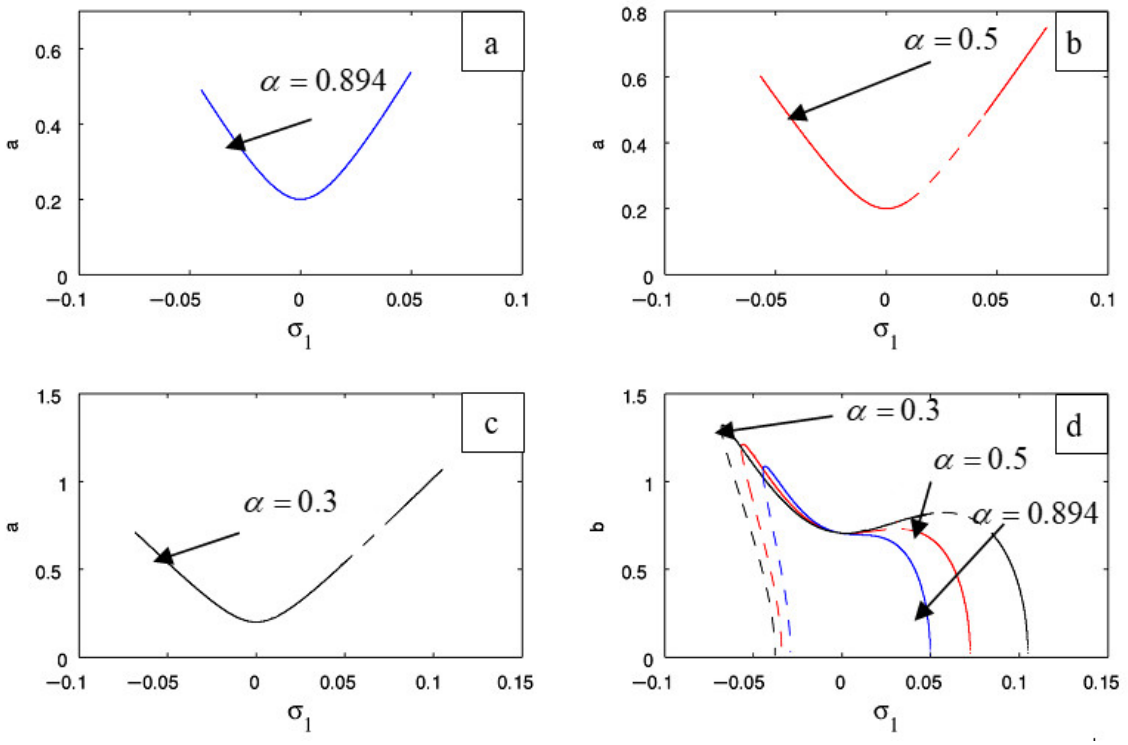

Figure 10. Effects of nonlinear parameter α: (a) the main system a; (b) NSC b.

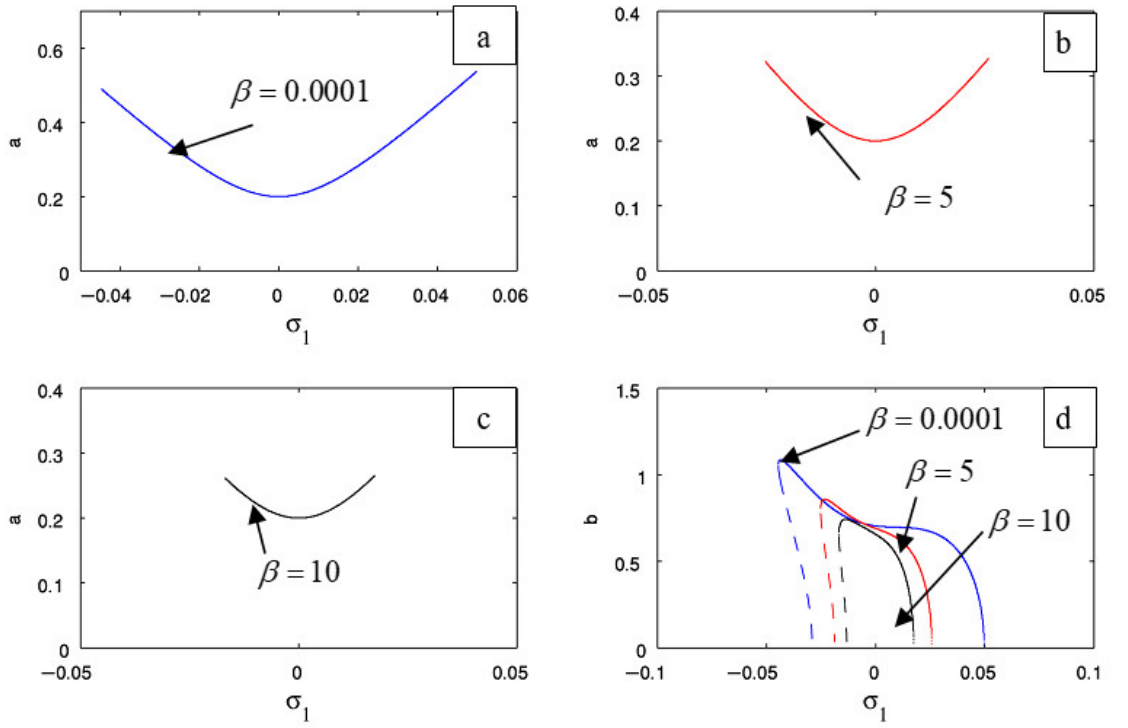

Figure 11. Effects of nonlinear parameter β: (a) the main system a; (b) NSC b.

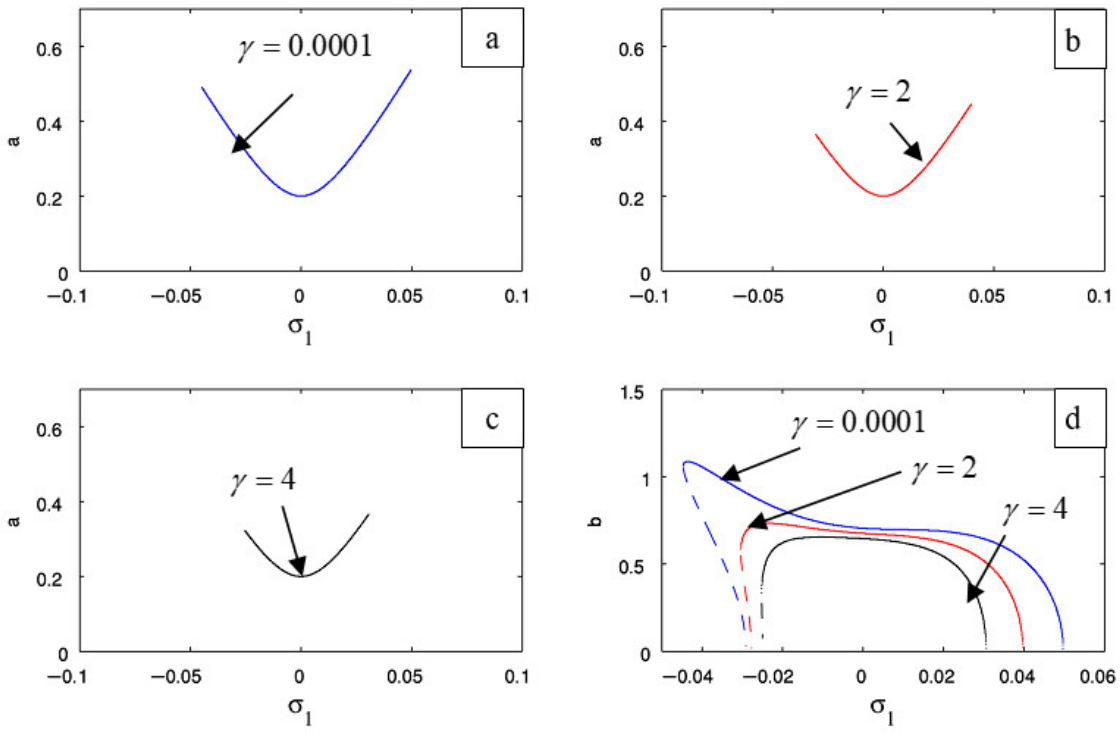

Figure 12. Effects of nonlinear parameter γ : (a) the main system a ; (b) NSC b .

4.1.5. Effect of control signal gain γ_1

Figure 13(a) appears that the amplitude of the system saturated like control signal gain γ_1 increased. Moreover, the amplitude of NSC is a monotonic decreasing function of control signal gain as shown in Figure 13(b).

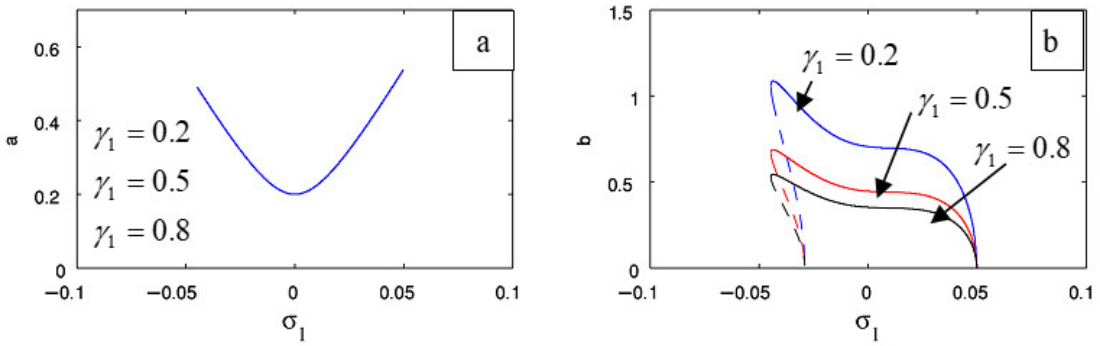

Figure 13. Effects of control signal gain γ_1 : (a) the main system a ; (b) NSC b .

4.1.6. Effect of feedback control gain γ_2

Figure 14 illustrates that for the large value of the feedback signal gain γ_2, the amplitudes of system and NSC increased. Furthermore, bandwidth for both steady state amplitude is wider.

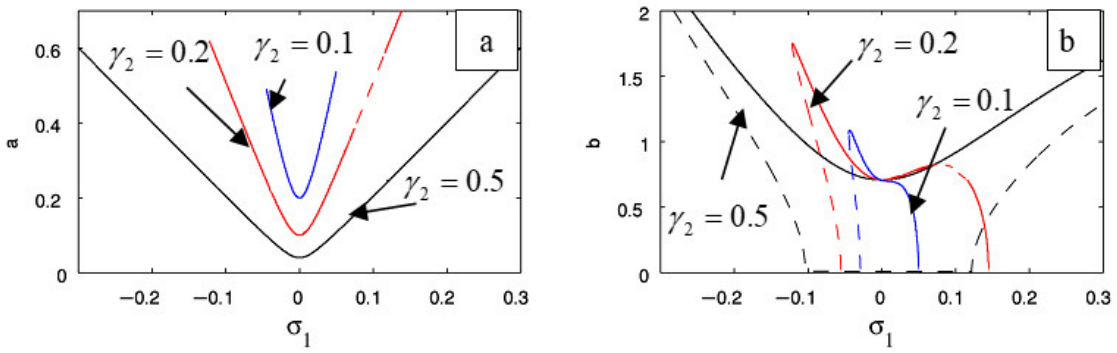

Figure 14. Effects of control signal gain γ_2: (a) the main system a; (b) NSC b.

4.1.7. Effect of detuning parameter σ_2

Figure 15 shows that once σ_2 increased, amplitudes of both head system and NSC decreased and shifted to the left. As of the frequency response curves, we obtained so as to the lowest amplitude of the system occurs at $\sigma_2 = 0.05, \sigma_2 = 0$ and $\sigma_2 = -0.05$ when $\sigma_1 = -0.05, \sigma_1 = 0$ and $\sigma_1 = 0.05$, respectively. This means that $\sigma_1 = -\sigma_2$.

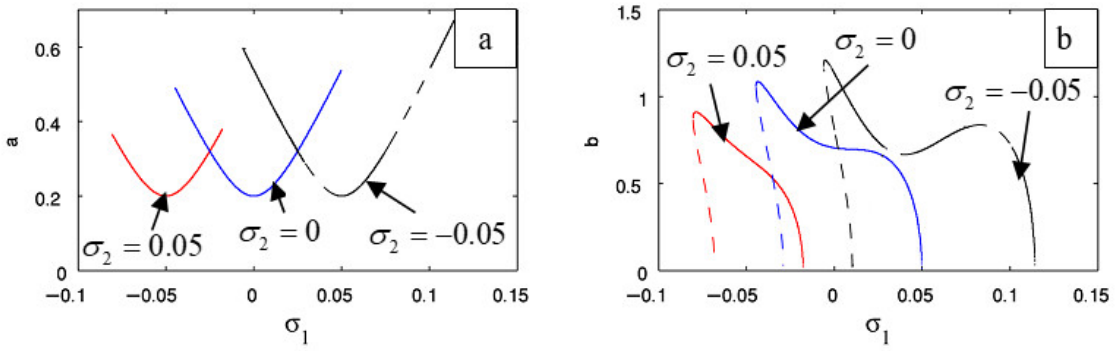

Figure 15. Effects of detuning parameter σ_2: (a) the main system a; (b) NSC b.

5. Verification of analytical solutions using numerical simulation solutions

The system which set by Eqs (2.2) and (2.3) solved numerically at the simultaneous primary in the presence 1:2 internal resonance case where ($\Omega \cong \omega_s$, $\omega_s \cong 2\omega_c$) compared with the analytical solution of the modulating Eqs (2.19) to (2.22) as presented in Figure 16. On the other hand, the continuous lines symbolize the time histories which obtained numerically (using RKM) for Eqs (2.2) and (2.3), and the dashed lines confirm inflection of amplitudes for the coordinates x and ν at similar values of parameters which using in Figure 3.

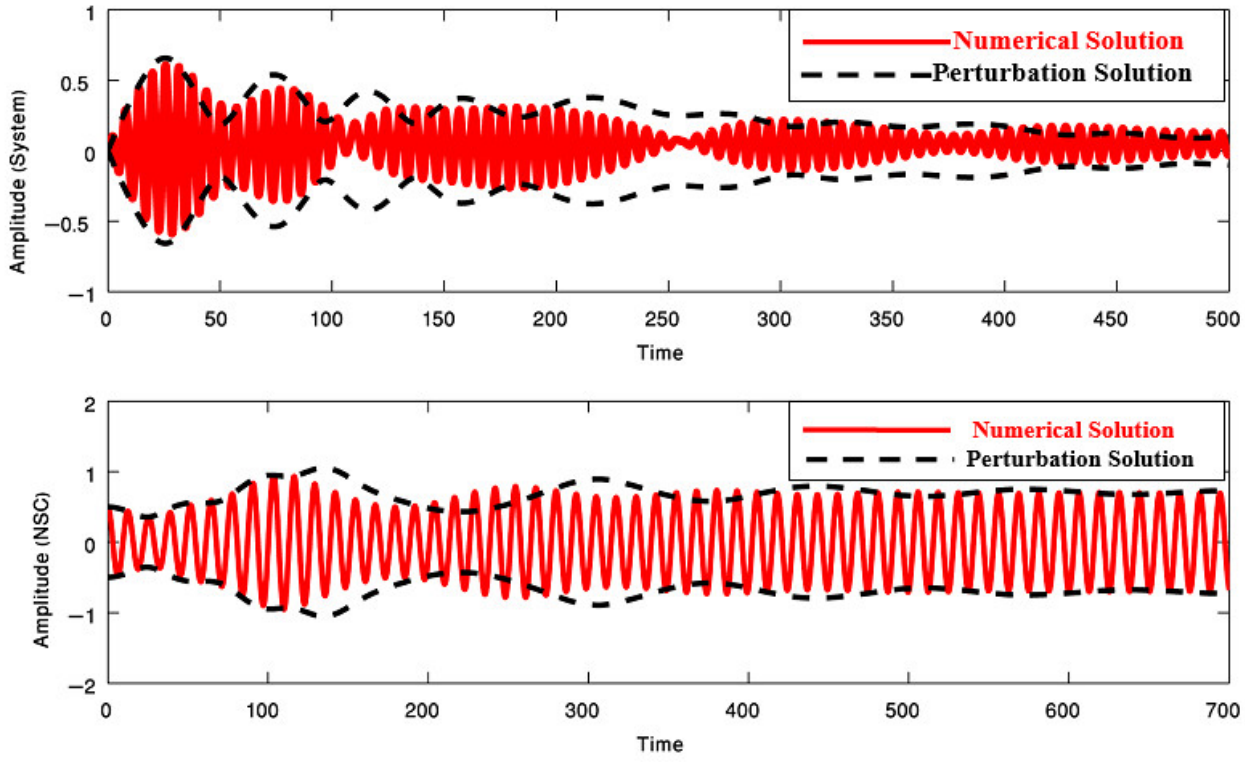

Figure 16. Relationship connecting numerical solution (using RKM) and mathematical solution (using perturbation method) of the system and NSC.

6. Comparison with previously published work

Reference [16] studied a harmonically excited dynamical system with a new NIPPF, IRC and PPF controllers. They studied the system with NIPPF analytically by using perturbation performance at primary and 1:1 internal resonance case. They can reduce the vibration amplitude, with zero initial conditions, by using NIPPF, PPF and IRC approximately to 84.87, 82.24, and 46.71%, respectively from its value of the uncontrolled system.

The subject in this article presents the nonlinear system with external excitation force to decrease vibrations by applying the nonlinear saturation controller (NSC). Perturbation technique useful to conclude the frequency response equations at primary and 1:2 internal resonance cases. We succeed to trim down the amplitude of the system, with nonzero initial conditions, approximately to 65.55% forms

its resonance value of the non-controlled system. From the study of the effect of parameters and stability regions, we obtained that we can reduce the amplitude by decreasing $\eta_c, \omega_s, \alpha, \beta$ and γ. The analysis demonstrates with the purpose of all calculation from the methodical solution is in excellent agreement with the numerical simulation.

7. Conclusions

A nonlinear saturation controller is proposed to improve the control performance of a dynamical cantilever beam system. The suggested nonlinear controller NSC has been studied for the main system with external excitation force near the considered simultaneous resonance case. According to the introduced control law, the system dynamical model is investigated and then analyzed utilizing perturbation techniques. Stability and the effects of some key parameters of the system are also examined numerically. The regions of stable and unstable of the controlled system are determined and recorded. The influence of the system dynamics with and without controller were explored through different response curves showing the regions of stable, unstable, saddle-node bifurcation, pitchfork bifurcation, and Hopf bifurcation. Finally, numerical confirmations for all obtained analytical results are introduced.

According to the above discussion, the following conclusions can be listed:

1). The measured resonance case is $\Omega \cong \omega_s$ and $\omega_s \cong 2\omega_c$ as the worst one.

2). The proposed control NSC method is main process for reducing the vibration amplitudes of the system dramatically.

3). The amplitude for the system reduced near 65.55 % as of its value without NSC. The saturation occurs for the main system and NSC at (t = 700 sec) and (t = 600 sec) correspondingly.

4). The amplitude of the system is monotonic increasing functions headed for the coefficients f, γ_1 and monotonic decreasing functions toward the parameters $\eta_c, \omega_s, \alpha, \beta$ and γ.

5). Using the saturation controller can avoid the phenomenon of double peaks on the frequency-response curve of the controlled system. Also, NSC can suppress the transient vibrations, thus shorten the time to reach a steady state and can also enhance the efficiency of the vibration reduction and suppress the nonlinear behavior of the system.

6). Both the steady state approximate solutions and the stability analysis based on the integral equation method are in excellent agreement with numerical simulations.

7). The response curves of the system before and after adding the saturation controller appeared various bifurcation phenomena.

Acknowledgments

We would like to thank the reviewers for their positive suggestions, which helped to improve the paper enormously.

Conflict of interest

The authors declare that there is no conflict of interest.

References

1. S. S. Oueini, A. H. Nayfeh, J. R. Pratt, A nonlinear vibration absorber for flexible structures, *Nonlinear Dyn.*, **15** (1998), 259–282. https://doi.org/10.1023/A:1008250524547
2. P. F. Pai, B. Wen, A. S. Naser, M. J. Schulz, Structural vibration control using PZT patches and non-linear phenomena, *J. Sound Vib.*, **215** (1998), 273–296. https://doi.org/10.1006/jsvi.1998.1612
3. S. S. Oueini, A. H. Nayfeh, Single-mode control of a cantilever beam under principal parametric excitation, *J. Sound Vib.*, **224** (1999), 33–47. https://doi.org/10.1006/jsvi.1998.2028
4. P. F. Pai, M. J. Schulz, A refined nonlinear vibration absorber, *Int. J. Mech. Sci.*, **42** (2000), 537–560. https://doi.org/10.1016/S0020-7403(98)00135-0
5. P. F. Pai, B. Rommel, M. J. Schulz, Non-linear vibration absorbers using higher order internal resonances, *J. Sound Vib.*, **234** (2000), 799–817. https://doi.org/10.1006/jsvi.1999.2896
6. O. N. Ashour, A. H. Nayfeh, Adaptive control of flexible structures using a nonlinear vibration absorber, *Nonlinear Dyn.*, **28** (2002), 309–322. https://doi.org/10.1023/A:1015622630382
7. L. Jun, H. X. Hua, R. Y. Shen, Saturation-based active absorber for a non-linear plant to a principal external excitation, *Mech. Syst. Signal Process.*, **21** (2007), 1489–1498. https://doi.org/10.1016/j.ymssp.2006.03.001
8. L. Jun, X. B. Li, H. X. Hua, Active nonlinear saturation-based control for suppressing the free vibration of a self-excited plant, *Commun. Nonlinear Sci. Numer. Simul.*, **15** (2010), 1071–1079. https://doi.org/10.1016/j.cnsns.2009.05.028
9. J. Xu, K. W. Chung, Y. Y. Zhao, Delayed saturation controller for vibration suppression in a stainless-steel beam, *Nonlinear Dyn.*, **62** (2010), 177–193. https://doi.org/10.1007/s11071-010-9708-4
10. A. T. EL-Sayed, Resonance behavior in coupled Van der Pol harmonic oscillators with controllers and delayed feedback, *J. Vib. Control*, **27** (2020), 1155–1170. https://doi.org/10.1177/1077546320938182
11. J. Warminski, M. Bochenski, W. Jarzyna, P. Filipek, M. Augustyniak, Active suppression of nonlinear composite beam vibrations by selected control algorithms, *Commun. Nonlinear Sci. Numer. Simul.*, **16** (2011), 2237–2248. https://doi.org/10.1016/j.cnsns.2010.04.055
12. N. A. Saeed, W. A. El-Ganini, M. Eissa, Nonlinear time delay saturation-based controller for suppression of nonlinear beam vibrations, *Appl. Math. Modell.*, **37** (2013), 8846–8864. https://doi.org/10.1016/j.apm.2013.04.010
13. Y. S. Hamed, S. K. Elagan, On the vibration behavior study of a nonlinear flexible composite beam under excitation forces via nonlinear active vibration controller, *Int. J. Basic Appl. Sci.*, **13** (2013), 9–18.
14. Y. S. Hamed, Y. A. Amer, Nonlinear saturation controller for vibration supersession of a nonlinear composite beam, *J. Mech. Sci. Technol.*, **28** (2014), 2987–3002. https://doi.org/10.1007/s12206-014-0706-1

15. M. Kamel, A. Kandil, W. A. El-Ganaini, M. Eissa, Active vibration control of a nonlinear magnetic levitation system via Nonlinear Saturation Controller (NSC), *Nonlinear Dyn.*, **77** (2014), 605–619. https://doi.org/10.1007/s11071-014-1323-3
16. E. Omidi, S. N. Mahmoodi, Sensitivity analysis of the nonlinear integral positive position feedback and integral resonant controllers on vibration suppression of nonlinear oscillatory systems, *Commun. Nonlinear Sci. Numer. Simul.*, **22** (2015), 149–166. https://doi.org/10.1016/j.cnsns.2014.10.011
17. J. C. Ji, N. Zhang, Suppression of the primary resonance vibrations of a forced nonlinear system using a dynamic vibration absorber, *J. Sound Vib.*, **329** (2010), 2044–2056. https://doi.org/10.1016/j.jsv.2009.12.020
18. J. C. Ji, N. Zhang, Suppression of super-harmonic resonance response using a linear vibration absorber, *Mech. Res. Commun.*, **38** (2011), 411–416. https://doi.org/10.1016/j.mechrescom.2011.05.014
19. J. C. Ji, Application of a weakly nonlinear absorber to suppress the resonant vibrations of a forced nonlinear oscillator, *J. Vib. Acoust.*, **134** (2012), 044502. https://doi.org/10.1115/1.4005839
20. J. C. Ji, Design of a nonlinear vibration absorber using three-to-one internal resonances, *Mech. Syst. Signal Process.*, **42** (2014), 236–246. https://doi.org/10.1016/j.ymssp.2013.06.019
21. H. S. Bauomy, A. T. El-Sayed, A new six-degrees of freedom model designed for a composite plate through PPF controllers, *Appl. Math. Modell.*, **88** (2020), 604–630. https://doi.org/10.1016/j.apm.2020.06.067
22. H. S. Bauomy, A. T. El-Sayed, Act of nonlinear proportional derivative controller for MFC laminated shell, *Phys. Scr.*, **95** (2020), 095210. https://doi.org/10.1088/1402-4896/abaa7c
23. H. S. Bauomy, A. T. El-Sayed, Mixed controller (IRC+NSC) involved in the harmonic vibration response cantilever beam model, *Meas. Control*, **53** (2020), 1954–1967. https://doi.org/10.1177/0020294020964243
24. A. T. El-Sayed, H. S. Bauomy, Outcome of special vibration controller techniques linked to a cracked beam, *Appl. Math. Modell.*, **63** (2018), 266–287. https://doi.org/10.1016/j.apm.2018.06.045
25. H. S. Bauomy, New controller (NPDCVF) outcome of FG cylindrical shell structure, *Alexandria Eng. J.*, **61** (2021), 1779–1801. https://doi.org/10.1016/j.aej.2021.06.061
26. J. C. Ji, X. Y. Li, L. Z. Zhang, Two–to–one resonant Hopf bifurcation in a quadratically nonlinear oscillator involving time delay, *Int. J. Bifurcation Chaos*, **22** (2012), 1250060. https://doi.org/10.1142/S0218127412500605
27. J. C. Ji, Secondary resonances of a quadratic nonlinear oscillator following two-to-one resonant Hopf bifurcations, *Nonlinear Dyn.*, **78** (2014), 2161–2184. https://doi.org/10.1007/s11071-014-1588-6
28. W. Zhang, J. Li, Global analysis for a nonlinear vibration absorber with fast and slow modes, *Int. J. Bifurcation Chaos*, **11** (2001), 2179–2194. https://doi.org/10.1142/S0218127401003334
29. W. Zhang, Chaotic motion and its control for nonlinear nonplanar oscillations of a parametrically excited cantilever beam, *Chaos, Solitons Fractals*, **26** (2005), 731–745. https://doi.org/10.1016/j.chaos.2005.01.042
30. W. Zhang, Z. Yao, M. Yao, Periodic and chaotic dynamics of laminated composite piezoelectric rectangular plate with one-to-two internal resonance, *Sci. China, Ser. E: Technol. Sci.*, **52** (2009), 731–742. https://doi.org/10.1007/s11431-009-0051-2

31. Y. X. Hao, W. Zhang, J. Yang, Nonlinear oscillations of a cantilever FGM rectangular plate based on third-order plate theory and asymptotic perturbation method, *Composites, Part B*, **42** (2011), 402–413. https://doi.org/10.1016/j.compositesb.2010.12.010
32. W. Zhang, M. H. Zhao, X. Y. Guo, Nonlinear responses of a symmetric cross-ply composite laminated cantilever rectangular plate under in-plane and moment excitations, *Compos. Struct.*, **100** (2013), 554–565. https://doi.org/10.1016/j.compstruct.2013.01.013
33. X. Y. Guo, W. Zhang, Nonlinear vibrations of a reinforced composite plate with carbon nanotubes, *Compos. Struct.*, **135** (2016), 96–108. https://doi.org/10.1016/j.compstruct.2015.08.063
34. S. F. Lu, Y. Jiang, W. Zhang, X. J. Song, Vibration suppression of cantilevered piezoelectric laminated composite rectangular plate subjected to aerodynamic force in hygrothermal environment, *Eur. J. Mech. - A/Solids*, **83** (2020), 104002. https://doi.org/10.1016/j.euromechsol.2020.104002
35. W. Zhang, G. Liu, B. Siriguleng, Saturation phenomena and nonlinear resonances of rotating pretwisted laminated composite blade under subsonic air flow excitation, *J. Sound Vib.*, **478** (2020), 115353. https://doi.org/10.1016/j.jsv.2020.115353
36. A. H. Nayfeh, *Perturbation Methods*, Wiley, New York, 2000. https://doi.org/10.1002/9783527617609
37. A. H. Nayfeh, D. Mook, *Nonlinear Oscillations*, Wiley, New York, 1995. https://doi.org/10.1002/9783527617586

Appendix

$$r_{11}=\left[-\frac{\eta_s}{2}\right], r_{12}=\left[\frac{f}{2\omega_s}\cos(\theta_{10})\right], r_{13}=\left[-\frac{\gamma_1}{2\omega_s}a_{20}\sin(\theta_{20})\right], r_{14}=\left[-\frac{\gamma_1}{4\omega_s}a_{20}^2\cos(\theta_{20})\right]$$

$$r_{21}=\left[\frac{\sigma_1}{a_{10}}-\left(\frac{9\alpha}{8\omega_s}+\frac{3\beta\omega_s}{8}-\frac{9\gamma\omega_s}{8}\right)a_{10}\right], r_{22}=\left[-\frac{f}{2a_{10}\omega_s}\sin(\theta_{10})\right], r_{23}=\left[\frac{\gamma_1 a_{20}}{2a_{10}\omega_s}\cos(\theta_{20})\right],$$

$$r_{24}=\left[-\frac{\gamma_1 a_{20}^2}{4a_{10}\omega_s}\sin(\theta_{20})\right]$$

$$r_{31}=\left[\frac{\gamma_2}{4\omega_c}a_{20}\sin(\theta_{20})\right], r_{32}=0, r_{33}=\left[-\frac{\eta_c}{2}+\frac{\gamma_2}{4\omega_c}a_{10}\sin(\theta_{20})\right], r_{34}=\left[\frac{\gamma_2}{4\omega_c}a_{10}a_{20}\cos(\theta_{20})\right]$$

$$r_{41}=\left[\frac{\gamma_2}{2\omega_c}\cos(\theta_{20})-\frac{\sigma_1}{a_{10}}+\left(\frac{9\alpha}{8\omega_s}+\frac{3\beta\omega_s}{8}-\frac{9\gamma\omega_s}{8}\right)a_{10}\right], r_{42}=\left[\frac{f}{2a_{10}\omega_s}\sin(\theta_{10})\right]$$

$$r_{43}=\left[\frac{(\sigma_2+\sigma_1)}{a_{20}}+\frac{\gamma_2}{2\omega_c a_{20}}a_{10}\cos(\theta_{20})-\frac{\gamma_1 a_{20}}{2a_{10}\omega_s}\cos(\theta_{20})\right],$$

$$r_{44}=\left[-\frac{\gamma_2 a_{10}}{2\omega_c}\sin(\theta_{20})+\frac{\gamma_1 a_{20}^2}{4a_{10}\omega_s}\sin(\theta_{20})\right]$$

$$\zeta_1=-r_{11}-r_{22}-r_{33}-r_{44}$$

$$\zeta_2=r_{33}r_{44}-r_{21}r_{12}+r_{11}r_{44}-r_{42}r_{24}+r_{11}r_{33}-r_{31}r_{13}-r_{41}r_{14}-r_{32}r_{23}-r_{34}r_{43}+r_{11}r_{22}+r_{22}r_{33}+r_{22}r_{44}$$

$$\begin{aligned}\zeta_3 = {} & r_{31}r_{12}r_{23} + r_{31}r_{13}r_{44} + r_{32}r_{23}r_{44} + r_{11}r_{32}r_{23} + r_{22}r_{34}r_{43} + r_{32}r_{43}r_{24} + r_{31}r_{43}r_{14} + r_{21}r_{12}r_{44} \\ & + r_{21}r_{12}r_{33} + r_{11}r_{42}r_{24} - r_{11}r_{22}r_{44} - r_{11}r_{22}r_{33} + r_{21}r_{32}r_{13} + r_{31}r_{22}r_{13} + r_{41}r_{12}r_{24} + r_{21}r_{42}r_{14} \\ & - r_{22}r_{33}r_{44} + r_{41}r_{14}r_{33} + r_{41}r_{13}r_{34} + r_{41}r_{22}r_{14} + r_{42}r_{23}r_{34} + r_{42}r_{24}r_{33} - r_{11}r_{33}r_{44} + r_{11}r_{34}r_{43}\end{aligned}$$

$$\begin{aligned}\zeta_4 = {} & r_{11}r_{22}r_{33}r_{44} - r_{11}r_{22}r_{34}r_{43} - r_{11}r_{32}r_{43}r_{24} - r_{11}r_{32}r_{23}r_{44} - r_{11}r_{42}r_{23}r_{34} - r_{11}r_{42}r_{24}r_{33} \\ & - r_{21}r_{12}r_{33}r_{44} + r_{21}r_{12}r_{34}r_{43} - r_{21}r_{32}r_{43}r_{14} - r_{21}r_{32}r_{13}r_{44} - r_{21}r_{42}r_{13}r_{34} - r_{21}r_{42}r_{14}r_{33} \\ & - r_{31}r_{12}r_{23}r_{44} - r_{31}r_{12}r_{43}r_{24} - r_{31}r_{22}r_{43}r_{14} - r_{31}r_{22}r_{13}r_{44} + r_{31}r_{42}r_{13}r_{24} - r_{31}r_{42}r_{23}r_{14} \\ & - r_{41}r_{12}r_{23}r_{34} - r_{41}r_{12}r_{24}r_{33} - r_{41}r_{22}r_{14}r_{33} - r_{41}r_{22}r_{13}r_{34} - r_{41}r_{32}r_{13}r_{24} + r_{41}r_{32}r_{23}r_{14}\end{aligned}$$

AIMS Press